Linear Frequency-Modulated Signal Detection Using Radon-Ambiguity Transform

Minsheng Wang, Andrew K. Chan, *Senior Member, IEEE*, and Charles K. Chui, *Fellow, IEEE*

***Abstract*— A novel time–frequency technique for linear frequency modulated (LFM) signal detection is proposed. The design of the proposed detectors is based on the Radon transform of the *modulus square* or the *envelope amplitude* of the ambiguity function (AF) of the signal. A practical assumption is made that the chirp rate is the only parameter of interest. Since the AF of LFM signals will pass through the origin of the ambiguity plane, the line integral of the Radon transform is performed over all lines passing through the origin of the ambiguity plane. The proposed detectors yield maxima over chirp rates of the LFM signals. This reduces the two-dimensional (2-D) problem of the conventional Wigner–Ville distribution (WVD) based detection or the Radon–Wigner transform (RWT) based detector to a one-dimensional (1-D) problem and consequently reduces the computation load and keeps the feature of "built-in" filtering. Related issues such as the finite-length effect, the resolution, and the effect of noise are studied. The result is a tool for LFM detection, as well as the time-varying filtering and adaptive kernel design for multicomponent LFM signals.**

I. Introduction

LINEAR frequency modulated (LFM) signals are frequently encountered in applications such as radar, sonar, seismic signal, etc. Detection of an LFM signal in a noise-free or high signal-to-noise environment is a relatively simple task. However, detection of multi-LFM signals in the presence of high level white noise requires techniques that are immutable to noise interferences. Time–frequency-based methods have attracted considerable attention and proven themselves to be effective among other techniques. Initial work based on the time–frequency analysis involved the spectrogram, which is the magnitude square of the short-time Fourier transform [5]. However, this technique suffers from the fixed time and frequency resolution due to the fixed window length used in the analysis and, therefore, limits its applications in practice. In [6] and [7], the wavelet transform is used because the wavelet transform does not have the fixed window limitation. On the other hand, the Wigner distribution (WD) has been found to be very useful for analyzing and detecting time-varying, nonstationary, phase-modulated signals [8]–[11]. In [12], an optimal WD-based detector was designed to detect LFM signals embedded in noise. The optimal detector was shown to be equivalent to quadrature matched filtering or the dechirp method [13]. For LFM signals, the WD detection algorithm computes the line integral of the WD along all lines in the time–frequency plane. The line that produces the maximum value corresponds to the maximum likelihood estimate of the linear instantaneous frequency of the chirp. This approach, which is known as the Radon–Wigner transform (RWT) [2], [3], turns the task of tracking straight lines in the time–frequency plane into locating maxima in a two-dimensional (2-D) (initial frequency versus chirp rate) plane. In practice, it is often the case that the chirp rate is the only parameter of interest [17]. In other words, the chirp rates distinguish different chirp signals. Such a scenario occurs in radar detection of a small fast moving missile launched from a relatively slow moving aircraft. Chirp signals can be detected by locating maxima in the chirp rate in many applications.

In this paper, we propose a Radon-ambiguity transform (RAT) that combines the ambiguity function (AF) [4] and Radon transform [2], [18] to detect multi-LFM signals in a noisy environment. The proposed approach reduces the detection of LFM signals to the location of maxima over chirp rates only. Two detectors are proposed: One is an envelope-based detector, and the other is a square-law-based detector. The performances such as the finite-length effect, the resolution, and the effect of noise are studied.

The organization of this paper is as follows: In Section II, the signal model is given, and its AF is calculated. By combining the AF and the Radon transform, the RAT detectors are introduced in Section III. A finite-length signal is discussed in Section IV. Section V analyzes the performance of both detectors. Computer simulations are given in Section VI to show the effectiveness of the proposed techniques. Discussions exploiting the relationships between the RAT and several correlated transforms are given in Section VII. Finally, Section VIII concludes the paper.

II. Signal Model and Ambiguity Function

The input signal to be analyzed is modeled by a linear sum of two (may be extended to more than two) LFM signals with chirp rates m_0 and m_1 as given by

$$r(t) = \sum_{i=0}^{1} e^{j[\omega_i t + (1/2)m_i t^2]}. \tag{1}$$

Here, ω_i represents the carrier (or the initial) frequencies that are proportional to the velocity of the target, and the chirp rate

Manuscript received November 20, 1995; revised August 25, 1997. This paper was supported in part by Texas Higher Education Coordinating Board Grant 999903-067 and Texas Instruments Grant C96-00356. The associate editor coordinating the review of this paper and approving it for publication was Dr. Bruce W. Suter.

The authors are with the Department of Electrical Engineering, Texas A&M University, College Station, TX 77843-3128 USA (e-mail: akchan@wavelet3.tamu.edu).

Publisher Item Identifier S 1053-587X(98)01994-1.

m_i is proportional to the acceleration. The AF defined by

$$\mathrm{AF}_r(\tau, \omega) = \int_{-\infty}^{\infty} r(t+\tau/2)r^{\star}(t-\tau/2)e^{-j\omega t}\,dt \qquad (2)$$

is computed for the signal $r(t)$ of (1) to yield

$$\begin{aligned}\mathrm{AF}_r(\tau, \omega) =& \delta(\omega - m_0\tau)e^{j\omega_0\tau} + \delta(\omega - m_1\tau)e^{j\omega_1\tau} \\ &+ e^{j\{[(\omega_0+\omega_1)/2]\tau+[(m_0-m_1)/8]\tau^2\}}Q_1 \\ &+ e^{j\{[(\omega_0+\omega_1)/2]\tau+[(m_1-m_0)/8]\tau^2\}}Q_2 \qquad (3)\end{aligned}$$

where we have (3a), shown at the bottom of the page. The last two terms of (3) are interference terms generated by the two LFM components in the signal $r(t)$, which are due to the nonlinearity of the AF. Using the identity [19]

$$\int_{-\infty}^{\infty} e^{-jmt^2}\,dt = \sqrt{\frac{\pi}{m}}\,e^{-j(\pi/4)}, \qquad m > 0 \qquad (4)$$

Q_1 and Q_2 are combined to give (5), also shown at the bottom of the page.

Fig. 1(a) shows the contour plot of the modulus of (5). Although there is cross term interference, we can identify the two straight lines representing the bicomponent signal in Fig. 1(a). However, the two LFM signals are not obvious if they are corrupted by the noise. Fig. 1(b) is identical to Fig. 1(a), except that the two signals with unit amplitudes are corrupted by Gaussian white noise with SNR $= -6$ dB. In order to detect the LFM signals in the noise background, we apply the Radon transform to the modulus of AF_r.

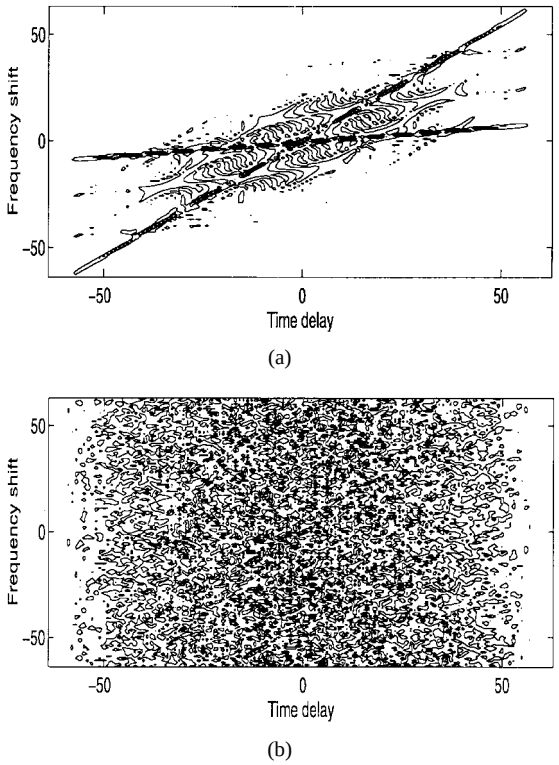

Fig. 1. AF's of a bicomponent LFM signal (a) without noise and (b) with the additive white Gaussian noise (SNR $= -6$ dB).

III. Radon-Ambiguity Transform

The Radon transform [3], which is commonly used for the reconstruction of images in computer tomography, is defined by

$$\begin{aligned}R_{s,\phi}\{f(x, y)\} =& \int_{-\infty}^{\infty}\int_{-\infty}^{\infty} f(x, y) \\ &\times \delta(x\sin\phi + y\cos\phi - s)\,dx\,dy \qquad (6)\end{aligned}$$

for $-\infty < s < \infty$ and $-(\pi/2) < \phi < \pi/2$, where the delta function specifies the direction of integration. The parameter s represents the shifted location of the origin. Equation (6) actually represents the sum of values of $f(x, y)$ along the line that makes an angle ϕ with the x axis and is located at a distance s from the origin. The RWT [2], [3] is a special case when $f(x, y)$ in (6) takes the WVD of a multicomponent LFM signal. The WVD of a bicomponent signal is graphically drawn in Fig. 2(a). The RWT of Fig. 2(a) should produce two maxima in the resulting α–ω plane. Fig. 2(b) is the AF of the same signal in Fig. 2(a). The AF is the 2-D Fourier transform of the WVD; thus they share the same angles of α_0 and α_1, as shown in the WVD. However, the initial frequencies shown in Fig. 2(a) have disappeared in Fig. 2(b) since they have been mapped into the phase of the AF. This also explains why the AF's of the two chirps pass through the origin in the τ–ξ plane. Thus, by applying the Radon transform to the *phase-free* AF, detection of multicomponent signals can be reduced from the 2-D search problem in the RWT to a one-dimensional (1-D) search problem. The advantage of the AF over the WVD has been shown in the kernel design for the time-frequency analysis [18]. This work is extended to the detection of multicomponent signals, and two different detectors are proposed by the authors.

Since all directions of interest pass through the origin of the ambiguity plane, the RT with parameter s set to 0 is applied to the phase-free AF of (5). We essentially compute the line integral along a straight line with its direction specified by the

$$\begin{aligned}Q_1 =& e^{-j\{[-2\omega+(m_0+m_1)\tau+2\omega_0-2\omega_1]^2/8(m_0-m_1)\}}\int_{-\infty}^{\infty} e^{j[(m_0-m_1)/2]\{t+[-2\omega+(m_0+m_1)\tau+2\omega_0-2\omega_1]/2(m_0-m_1)\}^2}\,dt \\ Q_2 =& e^{-j\{[-2\omega+(m_0+m_1)\tau+2\omega_1-2\omega_0]^2/8(m_1-m_0)\}}\int_{-\infty}^{\infty} e^{j[(m_1-m_0)/2]\{t+[-2\omega+(m_0+m_1)\tau+2\omega_1-2\omega_0]/2(m_1-m_0)\}^2}\,dt \qquad (3a)\end{aligned}$$

$$\begin{aligned}\mathrm{AF}_r(\tau, \omega) =& \delta(\omega - m_0\tau)e^{j\omega_0\tau} + \delta(\omega - m_1\tau)e^{j\omega_1\tau} + 2\sqrt{\frac{2\pi}{m_0 - m_1}} \\ &\times e^{j\{[\omega(\omega_0-\omega_1)+\omega_1 m_0\tau-\omega_0 m_1\tau]/(m_0-m_1)\}}\,\mathrm{Re}\left(e^{j\{[m_0 m_1\tau^2+\omega^2+(\omega_0-\omega_1)^2-\omega(m_0+m_1)\tau]/2(m_0-m_1)-\pi/4\}}\right) \qquad (5)\end{aligned}$$

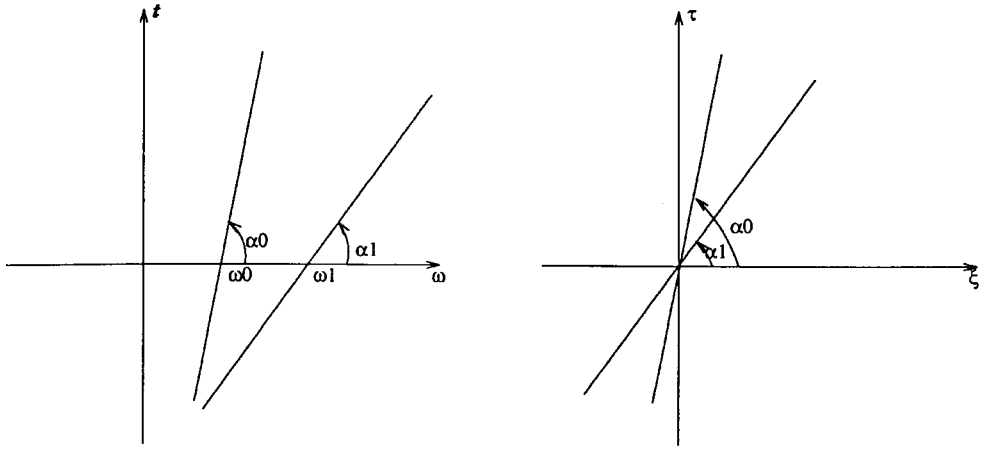

(a) (b)

Fig. 2. (a) WVD of a bicomponent signal and (b) the AF of the bicomponent signal. The AF is the 2-D Fourier transform of the WVD, and the initial frequency of the signal cannot be seen from the modulus of AF.

delta function $\delta(\xi - m\tau)$ in the ambiguity plane. Two detectors in RAT domain are shown in the following forms.

Modulus Square Detector:

$$\eta(m) = \int_{-\infty}^{\infty}\int_{-\infty}^{\infty} |\mathrm{AF}_r(\tau,\,\xi)|^2 \delta(\xi - m\tau)\, d\tau\, d\xi \quad (7)$$

$$= \int_{-\infty}^{\infty} |\mathrm{AF}_r(\tau,\, m\tau)|^2\, d\tau. \quad (8)$$

Envelope Detector:

$$\eta'(m) = \int_{-\infty}^{\infty}\int_{-\infty}^{\infty} |\mathrm{AF}_r(\tau,\,\xi)| \delta(\xi - m\tau)\, d\tau\, d\xi \quad (9)$$

$$= \int_{-\infty}^{\infty} |\mathrm{AF}_r(\tau,\, m\tau)|\, d\tau. \quad (10)$$

$\eta(m)$ is a measure of the performance of the detector as used in [4]. When $m = m_0$ or m_1, $\eta(m)$ should be large.

Since the infinite integrals of (8) and (10) usually diverge, it is necessary to first remove the constant term from the integrand. Specifically, for $m \neq m_i$ $(i = 0,\, 1)$ and assuming $m_0 - m_1 > 0$, we have from (5)

$$|\mathrm{AF}_r(\tau, m\tau)|^2 = \frac{8\pi}{m_0 - m_1}\cos^2(a_m\tau^2 + b) \quad (11)$$

$$= \frac{4\pi}{m_0 - m_1}[1 + \cos(2a_m\tau^2 + 2b)] \quad (12)$$

and

$$|\mathrm{AF}_r(\tau, m\tau)| = \left|2\sqrt{\frac{2\pi}{m_0 - m_1}}\cos(a_m\tau^2 + b)\right| \quad (13)$$

$$= 4\sqrt{\frac{2}{\pi(m_0 - m_1)}} \times \left[1 + \sum_{n=1}^{\infty}\frac{2(-1)^{n-1}}{(2n)^2 - 1}\cos(2na_m\tau^2 + 2nb)\right] \quad (14)$$

with

$$a_m = \frac{m_0 m_1 + m^2 - m(m_0 + m_1)}{2(m_0 - m_1)}$$

$$b = \frac{(\omega_0 - \omega_1)^2}{2(m_0 - m_1)} - \frac{\pi}{4}. \quad (15)$$

Removing the constants from (12) and (14) and substituting them into (8) and (10), respectively, yields

$$\eta(m) = \frac{4\pi}{m_0 - m_1}\sqrt{\frac{\pi}{a_m}}\sin\left(2b + \frac{\pi}{4}\right) \quad (16)$$

$$\eta'(m) = 4\sqrt{\frac{2}{a_m(m_0 - m_1)}}\sum_{n=1}^{\infty}\frac{2(-1)^{n-1}}{(2n)^2 - 1} \times \sqrt{\frac{1}{n}}\sin\left(2nb + \frac{\pi}{4}\right). \quad (17)$$

For $m \neq m_0$ or m_1 (i.e., $a_m \neq 0$), it is clear that $\eta(m)$ and $\eta'(m)$ are finite. By (15)–(17), we have $\eta(m) \to \infty$ and $\eta'(m) \to \infty$ as $m \to m_0$ or $m \to m_1$. Therefore, by calculating $\eta(m)$ or $\eta'(m)$ and comparing it with a preset threshold, the multicomponent signals can be detected. Performance and other related issues of the proposed two detectors are discussed in the following sections.

IV. Finite-Length Signal and Resolution

The signal used to illustrate the detection method so far has been assumed to be the infinite-length LFM signal in (1). Since realistic signals are of finite duration, it is necessary to examine the impact of signal length on the performance of the detectors. Both monocomponent and bicomponent signals are discussed.

Let $r(t)$ be a rectangular pulse having unity energy with time duration T.

$$r(t) = \begin{cases} \frac{1}{\sqrt{T}}\, e^{j[\omega_0 t + (1/2)m_0 t^2]} & \text{for } |t| \le \frac{T}{2} \\ 0 & \text{for } |t| > \frac{T}{2}. \end{cases} \quad (18)$$

The modulus of its AF is [20]

$$|\mathrm{AF}_r(\tau,\, \omega)| = \begin{cases} \left|\dfrac{\sin\left[\left(1 - \frac{|\tau|}{T}\right)\frac{T}{2}(\omega - m_0\tau)\right]}{\frac{T}{2}(\omega - m_0\tau)}\right| & \text{for } |\tau| \le T \\ 0 & \text{for } |\tau| > T. \end{cases} \quad (19)$$

The modulus square detector of (7) gives

$$\eta(m) = \frac{1}{T}\int_{-\infty}^{\infty}\int_{-\infty}^{\infty} |\mathrm{AF}_r(\tau,\omega)|^2 \delta(\omega - m\tau)\, d\tau\, d\omega \quad (20)$$

$$= \frac{2}{T^3}\int_0^T \left\{ \frac{\sin\left[(T-\tau)(m-m_0)\frac{\tau}{2}\right]}{(m-m_0)\frac{\tau}{2}} \right\}^2 d\tau. \quad (21)$$

The coefficient in front of the integral in (20) is added for normalization purposes. When m takes on the value of m_0, (21) yields

$$\eta(m_0) = \frac{2}{T^3}\int_0^T \lim_{p\to 0} \frac{\sin^2[(T-\tau)p\tau]}{(p\tau)^2}\, d\tau$$

$$= \frac{2}{T^3}\int_0^T (T-\tau)^2\, d\tau = 2/3. \quad (22)$$

For $m > m_0$, the variable in (21) is changed by letting $(m-m_0)/2 = p$ so that $\eta(m)$ is expressed by

$$\eta(2p+m_0) = \frac{2}{T^3}\int_0^T \frac{\sin^2[(T-\tau)p\tau]}{(p\tau)^2}\, d\tau$$

$$= \frac{2}{pT^2}\int_0^{T^2p/4} \frac{\sin^2(x)}{x^2}\, dx + \frac{4}{T^3}\int_{T/2}^T \frac{\sin^2[(T-\tau)p\tau]}{(p\tau)^2}\, d\tau. \quad (23)$$

Using the identity [19]

$$\int \frac{\sin^2(x)}{x^2}\, dx = si(2x) - \frac{\sin^2(x)}{x} \quad (24)$$

on the first term of (23) and by recalling the inequality

$$\int_{T/2}^T \frac{\sin^2[(T-\tau)p\tau]}{(p\tau)^2}\, d\tau < \frac{1}{p^2}\int_{T/2}^T \frac{1}{\tau^2}\, d\tau = \frac{1}{p^2T} \quad (25)$$

(23) becomes

$$\eta(2p+m_0) < \frac{2}{pT^2}\left[si\left(\frac{T^2}{2}p\right) - \frac{4}{pT^2}\sin^2\left(\frac{T^2}{4}p\right) + \frac{2}{pT^2}\right]. \quad (26)$$

By letting $2p + m_0 = m$, (26) is expressed as

$$\eta(m) < \frac{4}{(m-m_0)T^2}\left\{ si\left[\frac{T^2}{4}(m-m_0)\right] + \frac{4}{(m-m_0)T^2}\cos\left[\frac{T^2}{4}(m-m_0)\right]\right\} \quad (27)$$

where

$$si(x) = \int_0^x \frac{\sin(t)}{t}\, dt \quad (28)$$

is the integral of the sinc function.

Equations (22) and (27) give the upper bound of the modulus square detector of $\eta(m)$ for $m \geq m_0$. For $m < m_0$, $\eta(m+m_0)$ can be determined by $\eta(m) = \eta(-m+2m_0)$.

We remark here that normalization by $1/T$ in (20) makes $\eta(m)$ convergent. This normalization plays the same role as removing the constant from (12), which makes the application easier to implement.

The upper bound of $\eta'(m)$ is estimated in a similar way. The results are shown in (29) at the bottom of the page.

The details are given in Appendix A. Fig. 3 shows the upper bounds of $\eta(m)$ and $\eta'(m)$, as well as the graphs of $\eta(m)$ and $\eta'(m)$ for $T = 40$. One can see from this figure that our estimated bounds are quite accurate, especially for the $\eta(m)$. The 3-dB response widths of the $\eta(m)$ and $\eta'(m)$ can be estimated from (27) and (29). They are less than $8\pi/T^2$ and $16\pi/T^2$ for $\eta(m)$ and $\eta'(m)$, respectively. The 3-dB width is a measure of selectivity of a measuring device [21]. When T is infinite, both $\eta(m)$ and $\eta'(m)$ become delta functions, as discussed in the preceding sections.

Now, we consider a bicomponent finite-length signal as given by

$$r(t) = \begin{cases} \frac{1}{\sqrt{T}}\, e^{j[\omega_0 t + (1/2)m_0 t^2]} + \frac{1}{\sqrt{T}}\, e^{j[\omega_1 t + (1/2)m_1 t^2]} & \text{for } |t| \leq \frac{T}{2} \\ 0 & \text{for } |t| > \frac{T}{2} \end{cases} \quad (30)$$

with the assumption that $\omega_0 = \omega_1$ and $m_0 > m_1$ for simplicity purposes. The modulus of the AF of $r(t)$ for $\omega = m\tau$ can be calculated by making use of the integral [19]

$$\int e^{j(px^2+2qx)}\, dx = \sqrt{\frac{\pi}{2p}}\, e^{-j(q^2/p)}\left[C\left(\frac{px+q}{\sqrt{p}}\right) + jS\left(\frac{px+q}{\sqrt{p}}\right)\right] \quad (31)$$

to yield (32), shown at the bottom of the next page, where

$$C(x) = \int_0^x \cos\left(\frac{\pi t^2}{2}\right) dt$$

and

$$S(x) = \int_0^x \sin\left(\frac{\pi t^2}{2}\right) dt$$

$$\eta'(m) = \begin{cases} 1 & m = 0 \\ < \frac{4}{(m-m_0)T^2}\left\{ si\left[\frac{T^2}{8}(m-m_0)\right] + 2\ln 2\right\} & m \leq 8\pi/T^2 + m_0 \\ < \frac{4}{(m-m_0)T^2}\left(2\sum_{n=1}^{int[(m-m_0)T^2/8\pi]} (-1)^{n-1} si(n\pi) + (-1)^{int[(m-m_0)T^2/8\pi]}\, si\left\{ int\left[\frac{(m-m_0)T^2}{8\pi}\right]\pi\right\} + 2\ln 2\right) & m > 8\pi/T^2 + m_0 \\ \eta'(-m+2m_0) & m < m_0. \end{cases} \quad (29)$$

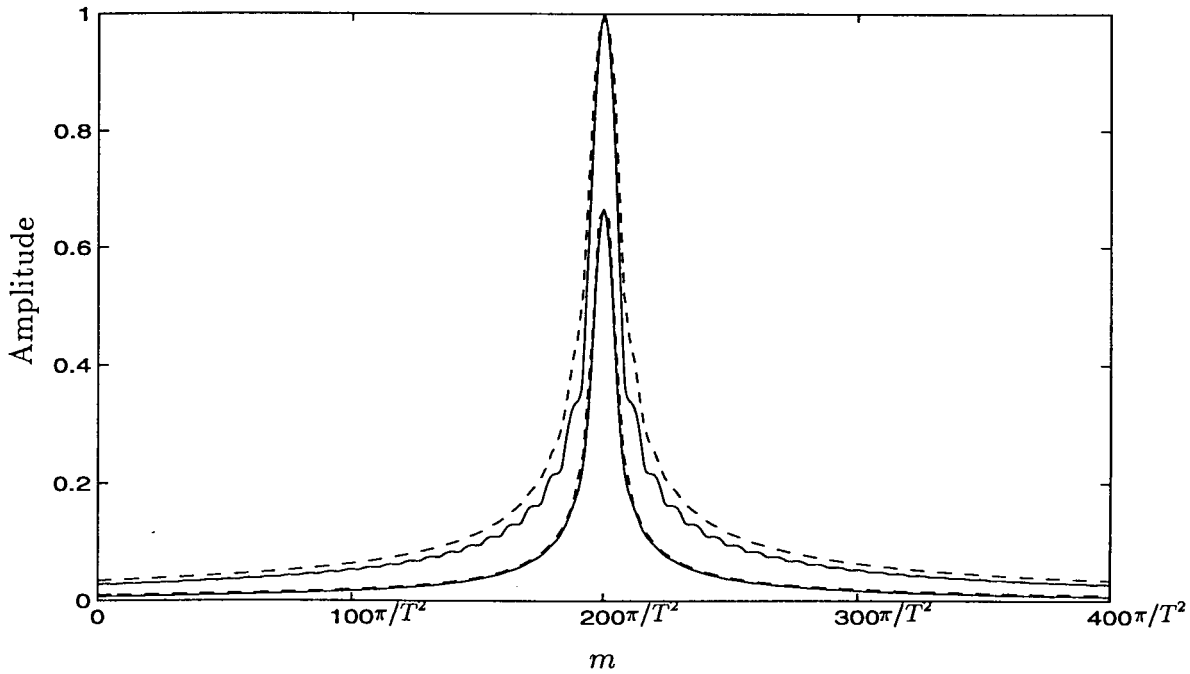

Fig. 3. Upper bounds of $\eta(m)$ and $\eta'(m)$, as well as the values of $\eta(m)$ and $\eta'(m)$ for $T = 40$. m_0 is chosen to be $200\pi/T^2$. Solid line inside: $\eta(m)$ when $T = 40$. Dashed line inside: upper bound of $\eta(m)$. Solid line outside: $\eta'(m)$ when $T = 40$. Dashed line outside: upper bound of $\eta'(m)$.

are the Fresnel integrals, and

$$X_0 = \sqrt{\frac{m_0 - m_1}{8}}\left[T + \frac{2(-m + m_1)}{m_0 - m1}\tau\right]$$
$$X_1 = \sqrt{\frac{m_0 - m_1}{8}}\left[T + \frac{2(m - m_0)}{m_0 - m1}\tau\right]$$

whereas a_m in (32) is defined by (15). For $|\tau| \leq T$, the first two terms in (32) represent the auto terms of the signal, whereas the rest express the cross term. On the other hand, we remark that (32) is similar to (13), corresponding to the case of the infinite signal, except that b in (13) is a constant while the corresponding terms in (32)—$[C(X_0)+C(X_1)]$ and $[S(X_0)+S(X_1)]$—are functions of m. Therefore, we can no longer expect an analytic solution to either $\eta(m)$ or $\eta'(m)$ for (32) as before, and the numerical method has to be used. Fig. 4 shows the integral of (32) and the integral of the square of (32) over τ, i.e., $\eta(m)$ and $\eta'(m)$. The integrals of the auto terms and cross terms of (32) are shown in Fig. 4.

Fig. 5 shows $\eta(m)$ and $\eta'(m)$ for a finite-length bicomponent signal with amplitude of one component being one third of the other. It can be concluded from Figs. 4 and 5 that the square-law detector is better for stronger or equal amplitude LFM signal detection, whereas the envelope detector is superior for weak chirp detection. This conclusion is straightforward since squaring any spectrum will increase its peakedness and consequently suppress the nondominant components.

Resolution, which is a commonly used parameter for measuring the ability to separate two chirp signals with a very small difference in chirp rate, has not been well defined. Rayleigh originally defined it as the minimum interval for which the resulting response still has the form of a double-humped curve [21]. This is too rough a definition to be of use here. In power spectrum estimation, the condition for two-sinusoid resolution used in [22] is that the response at the midpoint between the two components must be less than or equal to the average at the two components. This definition has two disadvantages: The minimum is not always the midpoint, and a slight shift in the location of the peak may produce a great difference in results. Other definitions in [23] and [24] have their own merits. In this application, resolution is defined as the minimum chirp rate separation necessary to resolve two equally strong LFM signals in a noise-free environment. Since the resolution depends on the signal length T, it might be

$$|\mathrm{AF}_r(\tau, m\tau)| = \begin{cases} \left| \dfrac{2\sin\left[(T-|\tau|)\dfrac{\tau}{2}(m-m_0)\right]}{T\tau(m-m_0)} + \dfrac{2\sin\left[(T-|\tau|)\dfrac{\tau}{2}(m-m_1)\right]}{T\tau(m-m_1)} + \dfrac{2}{T}\sqrt{\dfrac{\pi}{m_0-m_1}} \right. \\ \left. \quad \times \{[C(X_0)+C(X_1)]\cos(a_m\tau^2) + [S(X_0)+S(X_1)]\sin(a_m\tau^2)\} \right| & \text{for } |\tau| \leq T \\ 0 & \text{for } |\tau| > T \end{cases} \tag{32}$$

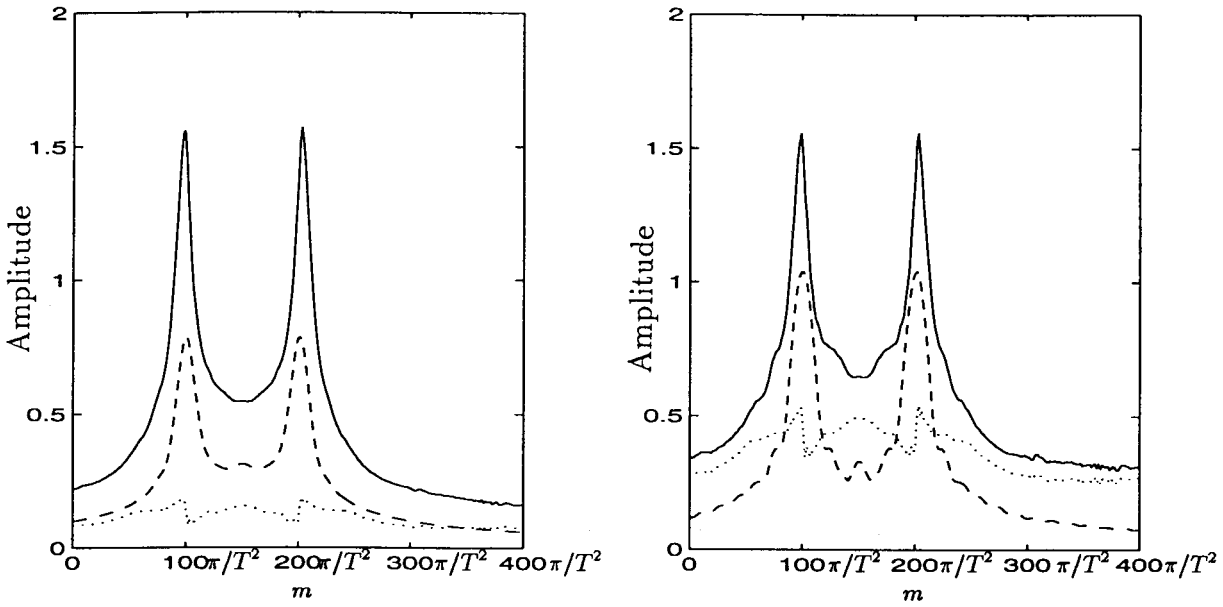

Fig. 4. $\eta(m)$ and $\eta'(m)$ of a bicomponent signal, $T = 40$, $m_0 = 200\pi/T^2$, $m_1 = 100\pi/T^2$: (a) $\eta(m)$. (b) $\eta'(m)$. Solid line: $\eta(m)$ or $\eta'(m)$. Dashed line: Auto terms only. Dotted line: Cross terms only.

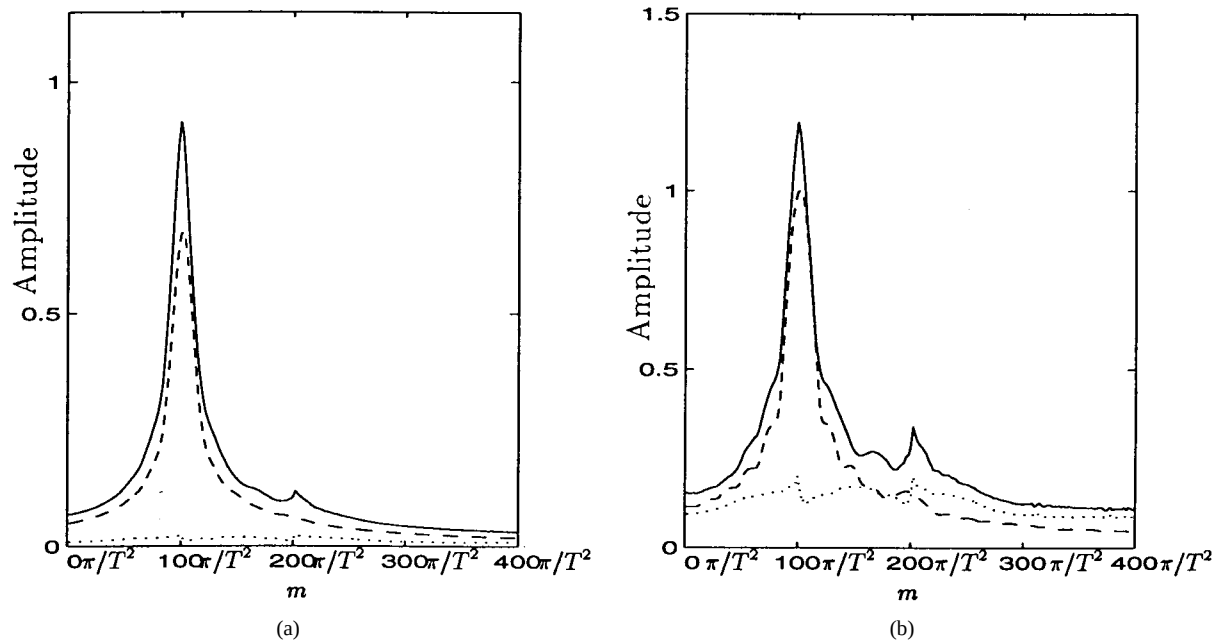

Fig. 5. $\eta(m)$ and $\eta'(m)$ of a bicomponent signal with the amplitude of one component being one third of the other $T = 40$, $m_0 = 200\pi/T^2$, $m_1 = 100\pi/T^2$. (a) $\eta(m)$ and (b) $\eta'(m)$. Solid line: $\eta(m)$ or $\eta'(m)$. Dashed line: Auto terms only. Dotted line: Cross terms only.

alternatively defined as the minimum signal length for a given chirp rate separation. The idea behind this definition is similar to that in [24], and the advantages are that it gives consistent results, and it does not depend on the value of $\eta(m)$ or $\eta'(m)$ at specific chirp rates.

Through computer simulations for trial signals with signal length T ranging from 5 to 50 at step 5, we get the resolutions to be about $1.5/T^2$ for $\eta(m)$ and $1.4/T^2$ for $\eta'(m)$. Fig. 6 shows the critically resolved cases of $\eta(m)$ and $\eta'(m)$ for $T = 40$. Taking $\eta(m)$, for example, when the frequency rate separation is less than $1.5/T^2$, such as $1.4/T^2$, the two peaks are merged, whereas when the separation becomes greater than $1.5/T^2$, the two peaks can be observed better and separated farther. Here, we admit that these resolutions are somehow subjective and optimistic, which results from the poor definition; however, they reveal that the resolution is adversely proportional to the square of the signal length T, as well as provide us with a lower bound for the signal length. Namely, the signal length must be greater than $\sqrt{1.5/\Delta}$ to achieve chirp rate resolution Δ. This is primary in the practical design. Recall that the frequency resolution of the Fourier transform is adversely proportional to the signal length,

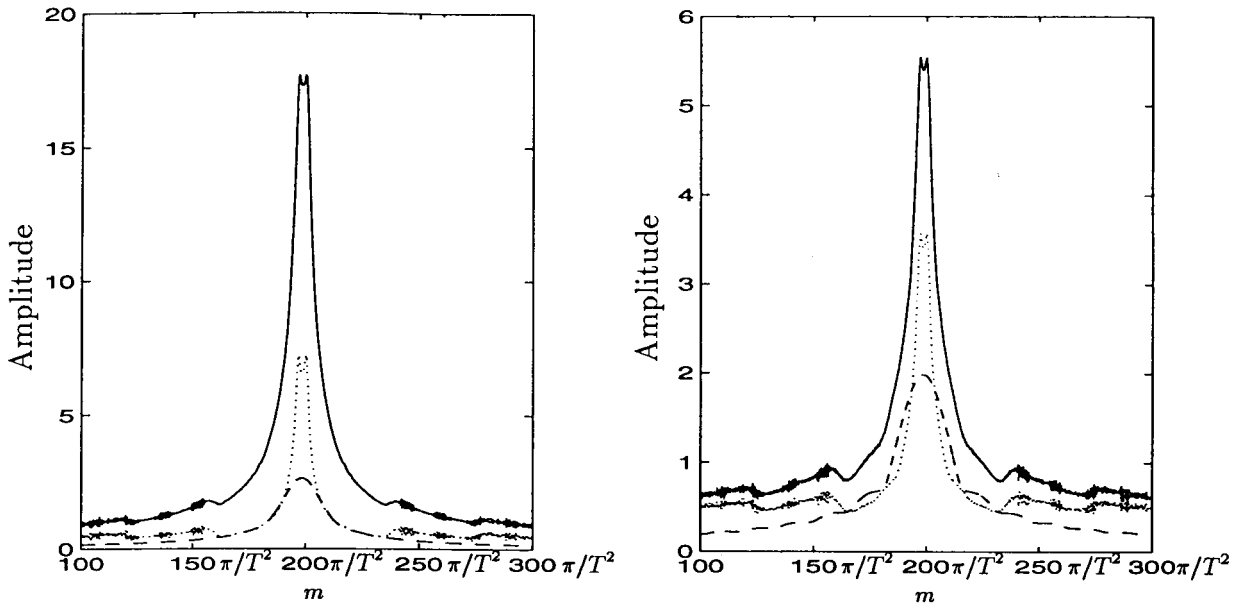

Fig. 6. Critical resolved cases of $\eta(m)$ and $\eta'(m)$, $T = 40$, $m_0 = 200\pi/T^2$. (a) $\eta(m)$, $m_1 = 198.5\pi/T^2$. (b) $\eta'(m)$, $m_1 = 198.6\pi/T^2$. Solid line: $\eta(m)$ or $\eta'(m)$. Dashed line: Auto terms only. Dotted line: Cross terms only.

whereas the chirp rate resolution here is adversely proportional to the square of the signal length. This is sensible since the phase of a chirp signal is linear to frequency and quadratic to chirp rate. In addition, note that the interference terms in Fig. 6 are much stronger than the auto terms for small chirp rate separation, which is justified by the third term of (32) when the difference between m_0 and m_1 is small. It is actually the interference terms rather than the auto terms that resolve different signals, as shown in Fig. 6. The fact that cross terms are important to resolution is not unique to the RAT; it is true in any of the bilinear transforms, including the Wigner transform and the RWT.

V. Performance Analysis

In this section, a performance comparison is made among the RWT detector, the envelope detector, and the square-law detector. The goal is to determine whether or not a signal is present at some time reference. A detection statistic η is formed, such that if η exceeds a certain threshold, the signal is considered to be present (hypothesis H_1). If not, it is decided that no signal is present (hypothesis H_0); that is, the recorded waveform corresponds to noise only. The noise is assumed to be a zero-mean, complex, white, stationary, Gaussian process of two-side power spectral density (PSD) N_0. The performance of a detection method can be characterized with the help of the performance SNR measure [1], [4], [42]

$$P(\text{SNR}) = \frac{|E(\eta|H_1) - E(\eta|H_0)|}{\{\frac{1}{2}[\text{var}(\eta|H_1) + \text{var}(\eta|H_0)]\}^{1/2}} \tag{33}$$

where $E(\eta|H_i)$ and $\text{var}(\eta|H_i)$ denote the expected value and variance of η, respectively, when $r(t)$ is the result of hypothesis H_i, $i = 0, 1$. Large SNR values indicate that the average values of η for the two hypotheses are well separated, whereas the variances of η are small. This characteristic results in improved detection.

The statistics of the RWT-based detection [2], [3] is

$$\eta_{\text{RW}}(\omega_0, m) = \int_{-\infty}^{\infty} W_r(t, \omega_0 + mt)\, dt \tag{34}$$

where W_r is the WD of the received signal. The performance SNR for this detector is

$$P(\text{SNR})_{\text{RW}} = \sqrt{\frac{A}{N_0}}\, \frac{1}{\sqrt{1 + \dfrac{N_0}{A}}} \tag{35}$$

where A is the energy of the reference signal $s(t)$ and N_0 is the PSD of the noise. The derivation of the $P(\text{SNR})_{\text{RW}}$ can be found in [1]. The $P(\text{SNR})$ of the matched filter detector is easily calculated to be $\sqrt{A/N_0}$, which is optimal between linear and nonlinear detectors. Comparing $P(\text{SNR})_{\text{RW}}$ with the optimal value of $\sqrt{A/N_0}$, we can see that $P(\text{SNR})_{\text{RW}}$ is scaled by a factor of $\sqrt{1/(1 + N_0/A)}$. For large value of A/N_0, $P(\text{SNR})_{\text{RW}}$ approaches $\sqrt{A/N_0}$. However, for small value of A/N_0, $P(\text{SNR})_{\text{RW}}$ degrades by $\sqrt{N_0/A}$. This degradation is due to its nonlinear transformation nature. Quite recently, a combined Wigner–Hough transform and its corresponding performance analysis was proposed [25]. Actually, it is identical to the dechirping implementation [13] of the RWT, except that a definition of SNR other than (33) is used in [25].

For calculation purposes as well as a comparison of performances, the means and variances of the statistics $\eta(m)$ and $\eta'(m)$ are derived. To do this, some high-order moment properties of the Gaussian process are first shown.

Suppose the random variables $\mathbf{x}_i$ are jointly Gaussian with zero mean, and $E\{\mathbf{x}_i\mathbf{x}_j\} = C_{ij}$. Then

$$E\{\mathbf{x}_1\mathbf{x}_2\mathbf{x}_3\mathbf{x}_4\} = C_{12}C_{34} + C_{13}C_{24} + C_{14}C_{23} \tag{36}$$

$$E\{\mathbf{x}_1\mathbf{x}_2\mathbf{x}_3\mathbf{x}_4\mathbf{x}_5\mathbf{x}_6\} = \sum_{i,j,k,l,m,n} C_{ij}C_{kl}C_{mn} \tag{37}$$

where

$$\{i, j, k, l, m, n\} \in [1, 2, 3, 4, 5, 6]^6$$
$$i < j,\ k < l,\ m < n$$
$$i < k < m,\ \ j \neq k,\ l \neq m$$

and

$$E\{\mathbf{x}_1\mathbf{x}_2\mathbf{x}_3\mathbf{x}_4\mathbf{x}_5\mathbf{x}_6\mathbf{x}_7\mathbf{x}_8\} = \sum_{i,j,k,l,m,n,p,q} C_{ij}C_{kl}C_{mn}C_{pq} \tag{38}$$

where

$$\{i, j, k, l, m, n, p, q\} \in [1, 2, 3, 4, 5, 6, 7, 8]^8$$
$$i < j,\ k < l,\ m < n,\ p < q$$
$$i < k < m < p,\ j \neq k$$
$$l \neq m,\ n \neq p.$$

Equation (36) can be found in [26], and the proofs of (37) and (38) are given in Appendix B. By using these properties, the following results for finite-length signals can be obtained.

$$\begin{aligned} E(\eta|H_0) &= E\left\{ \int_{-T}^{T} \frac{1}{2T} \left| \int_{-T}^{T} n\left(t+\frac{\tau}{2}\right) \right.\right. \\ &\quad \left.\left. \times\ n^*\left(t-\frac{\tau}{2}\right) e^{-jm\tau t}\, dt \right|^2 d\tau \right\} \\ &= \frac{1}{2T} \int_{-T}^{T}\int_{-T}^{T}\int_{-T}^{T} \\ &\quad \times E\Big[n\left(t+\frac{\tau}{2}\right) n^*\left(t-\frac{\tau}{2}\right) n^*\left(t_1+\frac{\tau}{2}\right) \\ &\quad \times n\left(t_1-\frac{\tau}{2}\right) e^{jm\tau(t_1-t)} \Big] dt\, dt_1\, d\tau \\ &= \frac{1}{2T} \int_{-T}^{T}\int_{-T}^{T} [N_0^2\delta(\tau) + N_0^2\delta(t)]\, dt\, d\tau = 2N_0^2 \end{aligned} \tag{39}$$

$$\begin{aligned} E(\eta|H_1) &= E\left\{ \int_{-T}^{T} \frac{1}{2T} \left| \int_{-T}^{T} \left[n\left(t+\frac{\tau}{2}\right) + s\left(t+\frac{\tau}{2}\right) \right] \right.\right. \\ &\quad \left.\left. \times \left[n^*\left(t-\frac{\tau}{2}\right) + s^*\left(t-\frac{\tau}{2}\right) \right] e^{-jm\tau t}\, dt \right|^2 d\tau \right\} \\ &= 2N_0^2 + 4AN_0 + A^2 \end{aligned} \tag{40}$$

$$\begin{aligned} \mathrm{var}(\eta|H_0) &= E\left\{ \int_{-T}^{T} \frac{1}{2T} \left| \int_{-T}^{T} n\left(t+\frac{\tau}{2}\right) \right.\right. \\ &\quad \left.\left. \times\ n^*\left(t-\frac{\tau}{2}\right) e^{-jm\tau t}\, dt \right|^2 d\tau - 2N_0^2 \right\}^2 \\ &= \frac{1}{(2T)^2} \int_{-T}^{T} \cdots \int_{-T}^{T} \\ &\quad \times E\Big[n\left(t+\frac{\tau}{2}\right) n^*\left(t-\frac{\tau}{2}\right) n^*\left(t_1+\frac{\tau}{2}\right) \\ &\quad \times n\left(t_1-\frac{\tau}{2}\right) n\left(t_2+\frac{\tau_1}{2}\right) n^*\left(t_2-\frac{\tau_1}{2}\right) \\ &\quad \times n^*\left(t_3+\frac{\tau_1}{2}\right) n\left(t_3-\frac{\tau_1}{2}\right) \\ &\quad \times\ e^{-jm\tau(t-t_1)} e^{-jm\tau_1(t_2-t_3)} \Big] \\ &\quad \times dt\, dt_1\, dt_2\, dt_3\, d\tau\, d\tau_1 - 4N_0^4 \\ &= 20N_0^4 \end{aligned} \tag{41}$$

$$\begin{aligned} \mathrm{var}(\eta|H_1) &= E\left\{ \int_{-T}^{T} \frac{1}{2T} \left| \int_{-T}^{T} \left[n\left(t+\frac{\tau}{2}\right) + s\left(t+\frac{\tau}{2}\right) \right] \right.\right. \\ &\quad \left.\left. \times \left[n^*\left(t-\frac{\tau}{2}\right) + s^*\left(t-\frac{\tau}{2}\right) \right] e^{-jm\tau t}\, dt \right|^2 d\tau \right. \\ &\quad \left. - (2N_0^2 + 4AN_0 + A^2) \right\}^2 \\ &= 20N_0^4 + 44AN_0^3 + 22A^2N_0^2 + 6A^3N_0. \end{aligned} \tag{42}$$

In the derivation of (39)–(42), T is assumed to be relatively large and the initial frequency of the signal zero. Using (39)–(42) on (33) yields

$$P(\mathrm{SNR})_\eta = \frac{A}{N_0} \frac{1 + \dfrac{4N_0}{A}}{\sqrt{3\dfrac{A}{N_0} + 11 + 22\dfrac{N_0}{A} + 20\left(\dfrac{N_0}{A}\right)^2}}. \tag{43}$$

The $P(\mathrm{SNR})$ of the $\eta'(m)$ can be derived similarly, which is given in Appendix C. The result is

$$P(\mathrm{SNR})_{\eta'} = \sqrt{\frac{A}{N_0}} \frac{1}{\sqrt{1 + \dfrac{N_0}{A}}}. \tag{44}$$

The derivation of (44) also assumes T to be relatively large and the initial frequency to be zero. Fig. 7 shows the $P(\mathrm{SNR})$'s of the envelope, the square law, and the RWT detector. Observant readers may have already noticed that the $P(\mathrm{SNR})$ of the $\eta'(m)$ in (44) is the same as that of RWT-based detector in (35). With the projection slice theorem [40], it is not surprising that the Radon–Wigner detection statistic and the envelope detector provide equivalent performance. Furthermore, with Moyal formula [41]

$$\begin{aligned} &\int_{-\infty}^{\infty}\int_{-\infty}^{\infty} W_r(t, \omega) W_s(t, \omega)\, dt\, d\omega \\ &\quad = 2\pi \left| \int_{-\infty}^{\infty} r(t) s^*(t)\, dt \right|^2 \end{aligned} \tag{45}$$

where $W_s(t, \omega)$ is the WD for the reference signal $s(t)$, we can easily prove that the square of RWT has the same expectation and variance as that of the ambiguity square-law detector and, therefore, has the equivalent $P(\mathrm{SNR})$ performance as seen in (43).

Equations (43) and (44) are derived under the ideal conditions that the signal length T is very large and the initial frequency of the signal is zero. In general, the $P(\mathrm{SNR})$ performances of the envelope detector and the square-law detector will be worse than that of the Wigner–Radon transform detector. The $P(\mathrm{SNR})$'s of envelope and Wigner–Radon detector approach A/N_0 for high-input SNR. At low-input SNR, the three detectors degrade greatly, illustrating a small-

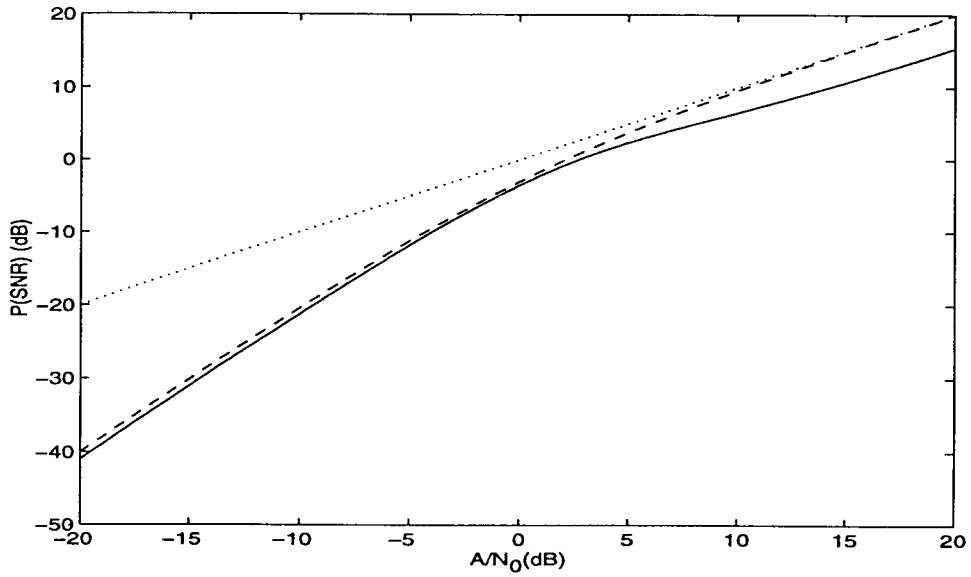

Fig. 7. Comparison between various $P(\text{SNR})$'s. Solid line: Square-law detector. Dashed line: Envelope detector or the RWT detector. Dotted line: $A/N_0 = 1$.

signal suppression effect typical of nonlinear detectors [43]. At high-input SNR, the square-law detector has a constant 5-dB performance loss. A detailed examination of (42) shows that it is comprised of the noise self-beat, which is the first term in (42) that is neglectable for high SNR, and the carrier-noise beats [44], which are the rest of the three terms in (42). At high SNR, these carrier-noise beats, especially the one represented by the last term in (42), contribute a lot and degrade the performance.

Another merit of performance commonly used in radar and communication system is output signal-to-noise ratio (SNR) [25], [36], [42]–[48]

$$\text{SNR}_{out} = \frac{\text{output signal power}}{\text{var}(\eta|H_1)} \tag{46}$$

which is the ratio between the output signal power and output noise power. For the coherent detector, SNR defined by (46) is equivalent (except the trivial square) to that by (33) because $\text{var}(\eta|H_1)$ and $\text{var}(\eta|H_0)$ are equal [45].

The SNR_{out} of the square-law detector can be easily calculated to be

$$\text{SNR}_{\eta} = \frac{\left(\frac{A}{N_0}\right)^2}{6\,\frac{A}{N_0} + 22 + 44\,\frac{N_0}{A} + 20\left(\frac{N_0}{A}\right)^2}. \tag{47}$$

The SNR_{out} of the envelope detector is

$$\text{SNR}_{\eta'} = \frac{\left(\frac{A}{N_0}\right)^2}{2\,\frac{A}{N_0} + 1} \tag{48}$$

which is the same as Wigner–Radon detector.

Fig. 8 shows the SNR_{out} of these detectors. For the high-input SNR, the envelope and Wigner–Radon detector has a 3-dB loss due to their bilinearity, and the square-law detector has an extra 5-dB loss due to its higher order of nonlinearity. For low-input SNR, the SNR_{out} performs worse than $P(\text{SNR})$ because the former ignores the effect of $\text{var}(\eta|H_0)$ and $E(\eta|H_0)$, as shown in (33). As pointed out in [46], although SNR is the most familiar criterion of merit of an information system, it is not necessarily an adequate measure of system performance. In addition, the definition of SNR for the nonlinear systems is ambiguous. In the definition of (33), a portion of cross term between the input signal and input noise [$4N_0/A$ in the numerator of (43)] is considered to be the signal, even though the SNR defined by (46) completely ignores the effect under hypothesis H_0. Other definitions of SNR can be found in [45]. When using SNR criterion, it is usually true that an increase in SNR improves the system, and consequently, it is worthwhile to know that one system provides how much higher one SNR is over another [46]. A very practical reason for using the SNR criterion is that it is the simplest measure of performance to evaluate analytically. Comparatively, the probability-based criterions require manipulations of the probability functions [49], [50]. We note that the matched filter detector is optimum under the above-mentioned SNR criterions as well as under the probability criterions such as likelihood ratio and inverse probability, provided the noise is a Gaussian random process [20], [36].

VI. Simulation Results

The detection methods introduced in the earlier sections are digitally simulated. Although there are some subtle differences between the continuous and discrete formulations of the WD, we treat the discretization as a sampling of the continuous WD's to be modeled. The following discrete LFM signal is used as the reference signal:

$$r(k) = e^{j(\pi/1024)k^2} + n(k), \qquad k = 1, 2, \cdots, 512 \tag{49}$$

where the complex noise $n(t)$ is generated by two independent, zero-mean, random processes with PSD N_0. Fig. 9 shows the outputs of $\eta(m)$ and $\eta'(m)$ with SNR's equal to ∞, -6 dB, and -9 dB, respectively.

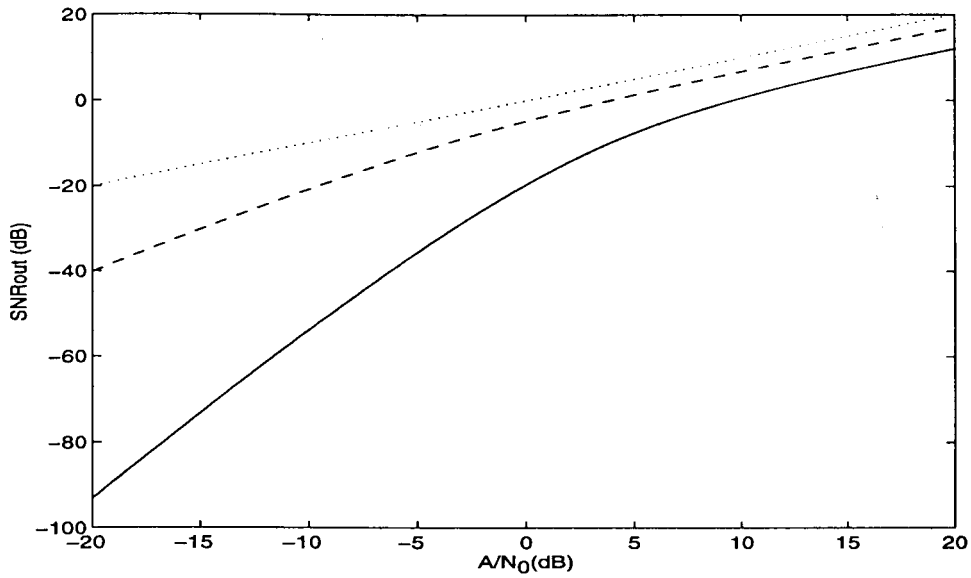

Fig. 8. Comparison between various SNR_{out}'s. Solid line: Square-law detector. Dashed line: Envelope detector or the RWT detector. Dotted line: $A/N_0 = 1$.

The second example is a multiple LFM signal of the form

$$r(k) = \sum_{i=0}^{3} e^{j[\omega_i + (m_i\pi/4096)k]k} + n(k) \qquad k = 1, 2, \cdots, 2048. \tag{50}$$

The following parameters of the signal were chosen to ensure that the maximum frequency of the signal is less than or equal to a quarter of the sampling frequency so that the resulting discrete WD is the properly sampled version of the desired continuous WD.

$$\omega_0 = 2\pi/1024, \quad \omega_1 = 10\pi/1024$$
$$\omega_2 = 6\pi/1024, \quad \omega_3 = 20\pi/1024 \tag{51}$$
$$m_0 = 0.124, \quad m_1 = 0.136$$
$$m_2 = 0.3, \quad m_3 = 0.5. \tag{52}$$

In fact, the maximum frequency of the above signal is just about one eighth of the sampling frequency. The outputs of the two detectors are shown in Fig. 10, with SNR's equal to ∞, -6 dB, and -12 dB, respectively. It can be seen from Fig. 10 that both detectors show the presence of the four LFM components under the strong noise background, with m_0 and m_1 being very close. These simulations have verified the effectiveness of the proposed detectors.

VII. Discussion

A. Comparison Between RAT and RWT

Letting $s(t) = e^{j[\omega_0 t + (1/2)mt^2]}$ represent the reference signal, the RWT-based detector (34) can be written as

$$\eta_{\mathrm{RW}}(\omega_0, m) = \int_{-\infty}^{\infty}\int_{-\infty}^{\infty} W_r(t, \omega) W_s(t, \omega)\, dt\, d\omega \tag{53}$$

where $W_s(t, \omega)$ is the WD for the reference signal, which is given by

$$W_s(t, \omega) = \delta(\omega - \omega_0 - mt). \tag{54}$$

Therefore, the detector $\eta_{\mathrm{RW}}(\omega_0, m)$ is the integration of the WVD of the received signal over all possible lines in the time–frequency plane. This search is computationally burdensome. Fortunately, the RWT can be calculated without prior calculation of the WD by a combination of time or frequency dechirping as [13]

$$\eta_{\mathrm{RW}}(\omega_0, m) = \left|\sqrt{2\pi}\int_{-\infty}^{\infty} r(t) e^{-j(1/2)mt^2}\, dt\right|^2. \tag{55}$$

The dechirping greatly reduces the computation of the RWT. However, the direct formulation of (53) would sometimes be useful since it allows an adaptive "built-in" time–frequency filtering [4]. Dechirping method can applied to WD as well as some non-WD such as Choi–Williams distribution. By the projection slice theorem, the Radon transform of any Cohen's class transforms can be calculated from the RWT by a one-dimensional convolution. This is performed by direct convolution along the frequency axis or by Fourier transformation into the ambiguity plane, multiplication by the polar representation of the ambiguity kernel, and transformation back to the Radon–Wigner plane. However, for the signal-dependant adaptive kernel, one cannot guarantee that the distribution modified by any kernel belongs to the Cohen's class; therefore, one has no way to apply dechirping to these distributions but to use the direct method of (53). This is the same as the issue of signal recovery from the time–frequency distribution, which one has to approximate the signal when an effective distribution is not available [4], [14]–[16].

Since the direct method must sometimes be used, a natural question would be if we can keep the adaptive time–frequency filtering feature while decreasing the computation. It can be shown that by making use of the AF, (53) can be written as [25], [28]

$$\eta_{\mathrm{RW}}(\omega_0, m) = \int_{-\infty}^{\infty} A_r(\tau, m\tau) e^{-j\omega_0\tau}\, d\tau. \tag{56}$$

Attention should be paid to the initial frequency ω_0. Once it was a variable of W_r in (34), but now, it appears in the phase function of the integrand in (56). It should be pointed out that although the line integral in (56) is performed over

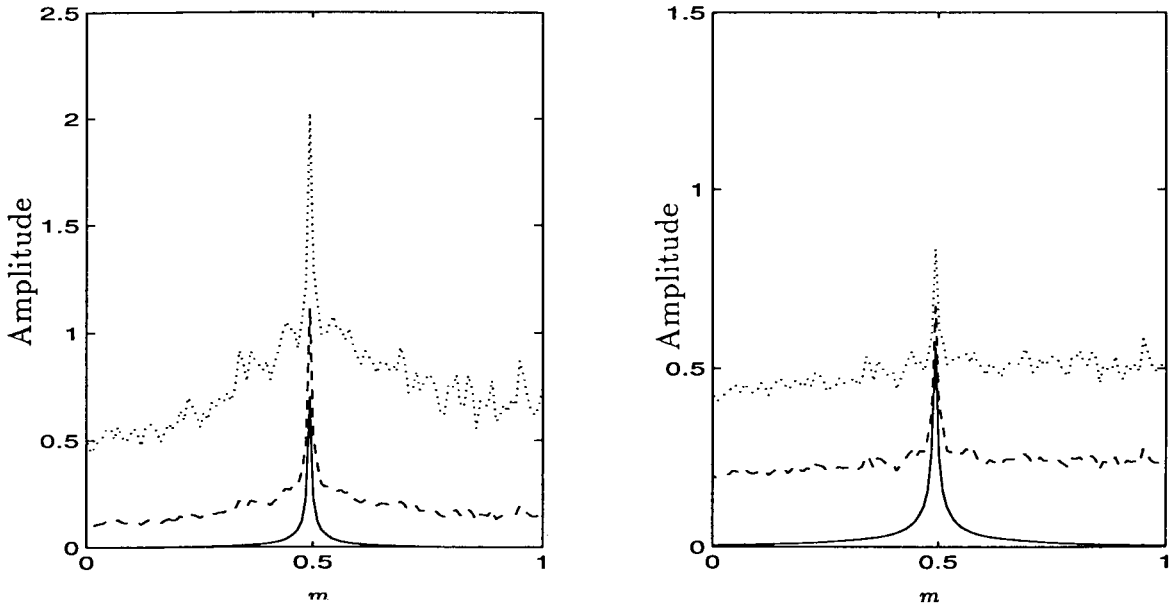

Fig. 9. $\eta(m)$ and $\eta'(m)$ of an LFM signal, $m_0 = 0.5$. (a) $\eta(m)$. (b) $\eta'(m)$. Solid line: SNR $= \infty$. Dashed line: SNR $= -6$ dB. Dotted line: SNR $= -9$ dB.

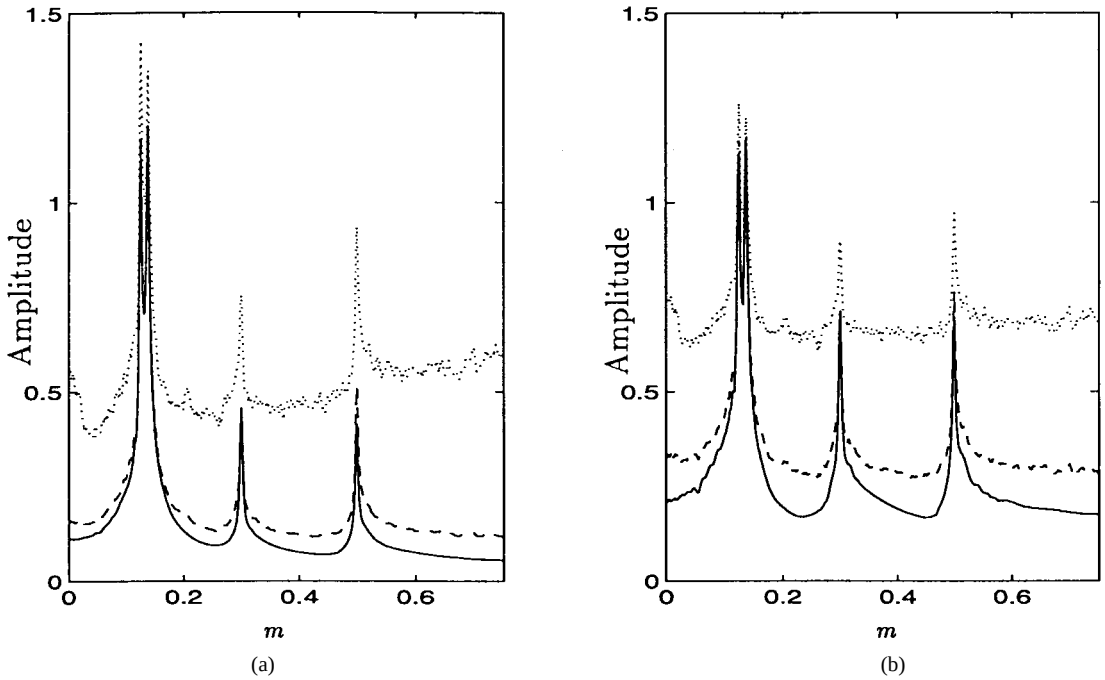

Fig. 10. $\eta(m)$ and $\eta'(m)$ of a tetracomponent signal $m_0 = 0.124$, $m_1 = 0.136$, $m_2 = 0.3$, $m_3 = 0.5$. (a) $\eta(m)$. (b) $\eta'(m)$. Solid line: SNR $= \infty$. Dashed line: SNR $= -6$ dB. Dotted line: SNR $= -12$ dB.

all lines passing through the origin of the ambiguity plane only, the computation of (56) is the same as that of (34), and one cannot expect to reduce the computation by (56). Under the practical assumption that the initial frequency ω_0 is trivial or at least not so important as m for detection, we get rid of it by taking modulus or modulus square of the AF. Our proposed detectors reduce the computation to a 1-D search problem, and we can modify the distribution by simply multiply (56) by any adaptive kernel without caring whether the resultant distribution is a Cohen's distribution. The properties and the performance analyzed in the preceding sections prove the reliability of the detectors. Incidentally, this 1-D RAT facilitates the detection.

It should be noted that although the RWT is referred to as a 2-D problem, it actually allows detection of chirp rates by simple linear search if one is not interested in the initial frequency w_0. Namely, one can compute the RWT of the signal, pick up the maxima of the RWT with respect to the angle, and linearly search these maxima [3]. One advantage of this technique is that as signal's energy becomes more concentrated near the chirp angles in the RWT, the median power in each projection falls, and the ratio of the $\mathrm{RWT}_{\max(r)}(r, \phi)/\mathrm{RWT}_{\mathrm{med}(r)}(r, \phi)$

appears to be more sensitive and robust than the $\mathrm{RWT}_{\max(r)}$ alone. Other measures of skewness may also differentiate chirps from background noise. In this respect, it is better than the RAT-based detector since the latter abandons the information of the initial frequency w_0.

1) Computational Requirements: Let N be the number of points in the signal and M the number of projection angles. M is in general slightly larger than N. Provided that the expensive trigonometric calls in chirp generation are avoided by precomputation, the cost of the RWT by dechirping is $O(NM \log_2 N)$ [2] and is primarily limited by the calculation of the fast Fourier transform. The computation of the RAT consists of the calculation of the AF, the transformation from the Cartesian coordinates to the polar coordinates, and the Radon transformation along the straight lines across the origin. The computation of AF is $O(N^2 \log_2 N)$, and the other two depend on the details of implementation. In general, dechirping is faster than the RAT. However, both computations are much less than that of the direct formulation of the RWT, which is $O(N^2M)$ [2]. Therefore, the RAT is not only more computationally efficient than the direct formulation of RWT but also allows for the potential application of adaptive time–frequency filtering [33].

2) Fractional Fourier Transform: The fractional Fourier transform (FRFT) is a generalization of the classical Fourier transform [34], [35]. It is a linear projection of the signal onto rotated frequency space. The FRFT is useful for time–frequency analysis because it allows an arbitrary rotation of the whole time–frequency plane. The Fourier transform is a special case of FRFT with the rotation angle equal to $\pi/2$. The Fourier transform is a first-order approximation of the signal frequency, which provides the information of the frequency for the pure sinusoid signal. The FRFT is a second-order approximation that provides the information of both initial frequency and the chirp rate for the LFM signal, whereas the Fourier transform smears the chirp rate into the frequency and results in the spread spectrum. If we do not care about the initial frequency, we use the RAT to achieve the almost equivalent performance to the FRFT or to the RWT.

The RWT is the magnitude-square of the FRFT. Bilinear methods have inherent disadvantages as well as advantages relative to linear detection schemes. The FRFT can be considered to be the correlation of the signal with the reference LFM signal; thus, its SNR is the same as the matched detector [1], which is $\sqrt{A/N_0}$. We see that the SNR of the RWT detector scales by a factor $\sqrt{1/(1+N_0/A)}$. For large values of A/N_0, this factor is approximately one, implying little difference between the use of the Radon–Wigner detector and the FRFT detector. On the other hand, values of A/N_0 that are much smaller than one yield a factor of approximately $\sqrt{A/N_0}$. Thus, for small input SNR, the performance of the Radon–Wigner detector degrades. This poor performance of the Radon–Wigner detector at small input SNR is due to its bilinear nature. For small input SNR, noise dominates the signal, and the bilinearity gives rise to further degradation.

3) Considerations on Potential Applications: Ristic and Boashash have applied the concept of the envelope detector to the kernel design [18]. The present work extends their contribution by providing a theoretical framework. The theoretical analysis has also shown that the square-law detector, which is a novel detector, has its merits. By the study of the finite length signal and the analysis of noise effect in Sections IV and V, we know that the detector to be used depends on the specific environment. Namely, when the signal under detection is stronger than or equal to the others, and the SNR is not too low, the square-law detector is preferred. For weak signals and bad noise environments, the envelope detector is better. This provides us with some guidelines for the potential application of the RAT to the time-varying filtering and adaptive kernel design.

It is well known that the AF and the WVD make up a 2-D Fourier transform pair; thus, by masking the kernel in the ambiguity domain, one can always suppress the interferences of the WVD. Various kernels are related to different distributions, such as the William–Choi distribution [29], STFT [30], and pseudo-WVD [31], etc. In [31], the author gives us a good explanation of why the distribution can suppress the cross terms. In fact, the kernel in [31] is a rectangular kernel. Appropriate masking in the ambiguity domain is equivalent to the smoothing in the time–frequency plane, which can suppress the interferences. This reminds us that the interferences of the AF can be suppressed in a similar way, and therefore, our detectors can be further improved. The idea is reasonable, but unfortunately, it cannot be implemented simply by multiplying a mask in the time–frequency plane, as is done in the kernel design. This is because the auto terms in the time–frequency plane do not have features as good as those appearing in the ambiguity domain, such as passage through the origin. Therefore, one cannot tell where the auto terms are and how to apply a mask. However, the wavelet packet transform or the filter banks [37]–[39] provide us with a tool to obtain a time–frequency distribution with low interference since the transform is adaptive to the signal. Once we get the time–frequency distribution, we can apply 2-D Fourier transform and obtain the AF, which is of low interference as well. In addition, by applying the RAT to the AF, better detection results can be achieved. This technique would be especially useful for the detection of weak LFM signals [33].

It is obvious that FRFT, the RWT, and the RAT are closely related, and they can be incorporated for our purpose. For example, in the application of inverse synthetic aperture radar (ISAR) [39], the received signal of the target can be considered to be a multicomponent LFM signal with each scatter represented by an LFM signal. One cannot get a clear image of all scatters by the conventional Fourier imaging technique because the Fourier transform spreads the spectrum of the LFM signal and, therefore, blurs the scatters. Our technique is to estimate the chirp rates of the multicomponent signal by the RAT and apply the FRFT to each signal with the rotation angle as the estimated chirp rate. Once the LFM signal has been corrected to a sinusoid signal, the conventional imaging method can be applied to get the focused image of this scatter. We apply this focusing to every dominant scatter of the target and finally get a clear image with all scatters being well focused.

VIII. Conclusions

Two kinds of multi-LFM detectors based on the RAT (the envelope detector and the square-law detector) have been proposed in this paper. A principle of the detector is that the AF's of LFM signals pass through the origin of the ambiguity plane. Thus, by applying the Radon transform to the AF, the multiple LFM signals embedded in the background noise can be detected. The resolution and the measurement accuracy of both detectors have been analyzed and are both inversely proportional to the square of the signal length. Performance analysis has shown that the square-law detector has its merit compared with the envelope and the RWT detector. Computer simulations have verified the effectiveness of the method.

Appendix A

The mathematical details of the upper bound estimate of the $\eta'(m)$ for the finite-length signal are given in this Appendix. Supplying (19) to (10) and letting $(m-m_0)/2=p$ yields

$$\eta'(2p+m_0)=\frac{2}{T^2}\int_0^T\left|\frac{\sin[(T-\tau)p\tau]}{p\tau}\right|d\tau. \tag{57}$$

Equation (57) is also normalized by multiplying the coefficient of $1/T$ as in (20). For $p=0$, (57) yields

$$\begin{aligned}\eta'(m_0)&=\frac{2}{T^2}\int_0^T\lim_{p\to 0}\frac{|\sin[(T-\tau)p\tau]|}{p\tau}\,d\tau\\&=\frac{2}{T^2}\int_0^T(T-\tau)\,d\tau=1.\end{aligned} \tag{58}$$

For $p\le 4\pi/T^2$, one has $0\le(T-\tau)p\tau\le\pi$, and

$$\begin{aligned}\eta'(2p+m_0)&=\frac{2}{T^2}\int_0^T\frac{\sin[(T-\tau)p\tau]}{p\tau}\,d\tau\\&=\frac{2}{T^2}\int_0^{T/2}\frac{\sin[(T-\tau)p\tau]}{(T-\tau)p\tau}(T-2\tau)\,d\tau\\&\quad+\frac{4}{T^2}\int_0^{T/2}\frac{\sin[(T-\tau)p\tau]}{p(T-\tau)}\,d\tau\\&=\frac{2}{pT^2}\int_0^{T^2p/4}\frac{\sin(x)}{x}\,dx\\&\quad+\frac{4}{T^2}\int_{T/2}^T\frac{\sin[(T-\tau)p\tau]}{p\tau}\,d\tau\\&<\frac{2}{pT^2}\left[si\left(\frac{T^2}{4}p\right)+2\ln 2\right].\end{aligned} \tag{59}$$

For $p>4\pi/T^2$, one has $(T-\tau)p\tau>\pi$, and the function $\sin[(T-\tau)p\tau]$ should have an even number of zeros, say, $2N$, in the interval $\tau\in[0,T]$, which are

$$\tau_n=\left(T-\sqrt{T^2-\frac{4n\pi}{p}}\right)\Big/2\qquad n=0,1,\cdots,N-1$$

and

$$\tau_n=\left[T+\sqrt{T^2-\frac{4(N-n)\pi}{p}}\right]\Big/2\qquad n=N+1,N+2,\cdots,2N. \tag{60}$$

It should be noted that $\tau_N=T/2$ is a zero only when $p=4k\pi/T^2$, where k is an odd number. By making use of the following relations between the zeros

$$T-\tau_{2N-n}=\tau_n=\left(T-\sqrt{T^2-\frac{4n\pi}{p}}\right)\Big/2\qquad\text{for } n=0,1,\cdots,2N \tag{61}$$

with

$$0=\tau_0<\tau_1<\cdots<\tau_{2N-1}<\tau_{2N}=T \tag{62}$$

we have

$$\begin{aligned}T^2\eta'(2p+m_0)=&\int_0^{\tau_1}\frac{\sin[(T-\tau)p\tau]}{p\tau}\,d\tau\\&-\int_{\tau_1}^{\tau_2}\frac{\sin[(T-\tau)p\tau]}{p\tau}\,d\tau\\&+\int_{\tau_2}^{\tau_3}(\cdot)\,d\tau-\int_{\tau_3}^{\tau_4}(\cdot)\,d\tau+\cdots\\&+\epsilon_N\int_{\tau_{N-1}}^{\tau_N}(\cdot)\,d\tau+\epsilon_N\int_{T-\tau_N}^{T-\tau_{N-1}}(\cdot)\,d\tau\\&+\cdots-\int_{T-\tau_2}^{T-\tau_1}(\cdot)\,d\tau+\int_{T-\tau_1}^{T}(\cdot)\,d\tau\end{aligned} \tag{63}$$

where

$$\epsilon_N=\begin{cases}1 & N\text{ is odd}\\ -1 & N\text{ is even.}\end{cases}$$

Note that since

$$\begin{aligned}&\int_{\tau_{n-1}}^{\tau_n}\frac{\sin[(T-\tau)p\tau]}{p\tau}\,d\tau-\int_{T-\tau_n}^{T-\tau_{n-1}}\frac{\sin[(T-\tau)p\tau]}{p\tau}\,d\tau\\&\quad=\frac{1}{p}\int_{(n-1)\pi}^{n\pi}\frac{\sin x}{x}\,dx\\&\quad=\frac{1}{p}[si(n\pi)-si((n-1)\pi)]\\&\quad n=1,2,\cdots,N\end{aligned} \tag{64}$$

and

$$\begin{aligned}&\epsilon_N\int_{T-\tau_N}^{T-\tau_{N-1}}(\cdot)d\tau+\cdots-\int_{T-\tau_2}^{T-\tau_1}(\cdot)d\tau+\int_{T-\tau_1}^{T}(\cdot)d\tau\\&\quad\le\int_{T-\tau_N}^{T-\tau_{N-1}}\frac{1}{p\tau}d\tau+\cdots+\int_{T-\tau_2}^{T-\tau_1}\frac{1}{p\tau}d\tau+\int_{T-\tau_1}^{T}\frac{1}{p\tau}d\tau\\&\quad=\int_{T-\tau_N}^{T}\frac{1}{p\tau}d\tau\\&\quad=\frac{1}{p}\ln 2\end{aligned} \tag{65}$$

we have

$$\eta'(2p+m_0)<\frac{2}{pT^2}\left[2\sum_{n=1}^{N}(-1)^{n-1}si(n\pi)+(-1)^N si(N\pi)+2\ln 2\right]. \tag{66}$$

Using the relation between N and p

$$T^2 - \frac{4N\pi}{p} \geq 0 \text{ or } N \leq \frac{pT^2}{4\pi} \tag{67}$$

we obtain

$$\begin{aligned}\eta'(2p+m_0) &< \frac{2}{pT^2}\left\{2\sum_{n=1}^{int[pT^2/4\pi]}(-1)^{n-1}si(n\pi)\right.\\ &\left.+(-1)^{int[pT^2/4\pi]}si\left(int\left[\frac{pT^2}{4\pi}\right]\pi\right)+2\ln 2\right\}. \end{aligned}\tag{68}$$

Equations (58), (59), and (68) together give (29), and the graph of this bound is shown in Fig. 3.

Appendix B

In this Appendix, we give the proofs for (37) and (38). Since the random variables $\mathbf{x}_i$ are jointly Gaussian, from the definition of joint normality, it follows that the random variable

$$\omega_1\mathbf{x}_1+\cdots+\omega_n\mathbf{x}_n \tag{69}$$

is normal, and therefore [26]

$$\begin{aligned}E\{e^{j(\omega_1\mathbf{x}_1+\cdots+\omega_n\mathbf{x}_n)}\} &= \exp\left\{-\tfrac{1}{2}\sum_{i,j}\omega_i\omega_jC_{ij}\right\}\\ &= \exp\left\{-\sum_{i=1,\,j;j=2,\,n}\omega_i\omega_jC_{ij}\right\}\end{aligned}\tag{70}$$

where $C_{ij}=E\{\mathbf{x}_i\mathbf{x}_j\}$. We expand the exponentials on the left and right sides of (70) and show explicitly only the terms containing the factor and $\omega_1\cdots\omega_8$

$$\begin{aligned}&E\{e^{j(\omega_1\mathbf{x}_1+\cdots+\omega_8\mathbf{x}_8)}\}\\ &\quad=\cdots+\frac{1}{8!}E\{(\omega_1\mathbf{x}_1+\cdots+\omega_8\mathbf{x}_8)^8\}+\cdots\\ &\quad=\cdots+\frac{8!}{8!}E\{\mathbf{x}_1\cdots\mathbf{x}_8\}\,\omega_1\cdots\omega_8\\ &\exp\left\{-\sum_{i=1,\,j;j=2,\,n}\omega_i\omega_jC_{ij}\right\}\\ &\quad=\cdots+\frac{1}{4!}\left(\sum_{i=1,\,j;j=2,\,n}\omega_i\omega_jC_{ij}\right)^4+\cdots\\ &\quad=\cdots+\frac{4!}{4!}\left(\sum_{i,j,k,l,m,n,p,q}C_{ij}C_{kl}C_{mn}C_{pq}\right)\omega_1\cdots\omega_8.\end{aligned}$$

Equating the corresponding coefficients, we obtain (38). Equation (37) can be proved similarly.

Appendix C

In order to derive the mean and variance of $\eta'(m)$, we prove that the random process

$$x_\tau(t)=n\left(t+\frac{\tau}{2}\right)n^*\left(t-\frac{\tau}{2}\right)e^{-jm\tau t} \tag{71}$$

is mean ergodic and cross covariance ergodic with the random process $x_{\tau_1}(t)$. Since the mean of $x_\tau(t)$ is

$$\begin{aligned}E\{x_\tau(t)\} &= E\left\{n\left(t+\frac{\tau}{2}\right)n^*\left(t-\frac{\tau}{2}\right)e^{-jm\tau t}\right\}\\ &= N_0\delta(\tau)\end{aligned}\tag{72}$$

and the cross variance is

$$\begin{aligned}C_{x_\tau(t)}(\theta) &= E\left\{\left[n\left(t+\frac{\tau}{2}\right)n^*\left(t-\frac{\tau}{2}\right)e^{-jm\tau t}\right]\right.\\ &\quad\left.\times\left[n^*\left(t+\theta+\frac{\tau}{2}\right)n\left(t+\theta-\frac{\tau}{2}\right)e^{jm\tau(t+\theta)}\right]\right\}\\ &\quad-E^2\{x_\tau(t)\}\\ &= N_0^2\delta(\theta)\end{aligned}\tag{73}$$

it follows from (73) that

$$\lim_{T\to\infty}\frac{1}{T}\int_0^T C_{x_\tau(t)}(\theta)\,d\theta=0. \tag{74}$$

Hence, the process $x(t)$ is mean ergodic [26]; therefore

$$\begin{aligned}&\lim_{T\to\infty}\frac{1}{2T}\int_{-T}^{T}n\left(t+\frac{\tau}{2}\right)n^*\left(t-\frac{\tau}{2}\right)e^{-jm\tau t}\,dt\\ &\quad=E\left\{n\left(t+\frac{\tau}{2}\right)n^*\left(t-\frac{\tau}{2}\right)e^{-jm\tau t}\right\}\\ &\quad=N_0\delta(\tau).\end{aligned}\tag{75}$$

The crosscovariance ergodicity can be proved similarly, and it follows that

$$\lim_{T\to\infty}\frac{1}{2T}\int_{-T}^{T}x_\tau(t)x_{\tau_1}^*(t-\alpha)\,dt=E[x_\tau(t)x_{\tau_1}^*(t-\alpha)]. \tag{76}$$

From (10), $\eta'(m)$ can be written as

$$\eta'(m)=\int_{-T}^{T}\left|\frac{1}{2T}\int_{-T}^{T}r\left(t+\frac{\tau}{2}\right)r^*\left(t-\frac{\tau}{2}\right)e^{-jm\tau t}\,dt\right|d\tau. \tag{77}$$

Supposing that the pulse width of T is relatively large and the initial frequency is zero, applying (75) to (77) yields

$$\begin{aligned}E(\eta|H_0) &= E\left\{\int_{-T}^{T}\left|\frac{1}{2T}\int_{-T}^{T}n\left(t+\frac{\tau}{2}\right)\right.\right.\\ &\quad\left.\left.\times\,n^*\left(t-\frac{\tau}{2}\right)e^{-jm\tau t}\,dt\right|d\tau\right\}\\ &= E\left\{\int_{-T}^{T}N_0\delta(\tau)\,d\tau\right\}=N_0\end{aligned}\tag{78}$$

$$\begin{aligned}E(\eta|H_1) &= E\left\{\int_{-T}^{T}\left|\frac{1}{2T}\int_{-T}^{T}\left[n\left(t+\frac{\tau}{2}\right)+s\left(t+\frac{\tau}{2}\right)\right]\right.\right.\\ &\quad\left.\left.\times\left[n^*\left(t-\frac{\tau}{2}\right)+s^*\left(t-\frac{\tau}{2}\right)\right]e^{-jm\tau t}\,dt\right|d\tau\right\}\\ &= A+N_0.\end{aligned}\tag{79}$$

$$\begin{aligned}\mathrm{var}(\eta|H_0) &= E\left\{\int_{-T}^{T}\left|\frac{1}{2T}\int_{-T}^{T} n\Big(t+\frac{\tau}{2}\Big)n^*\Big(t-\frac{\tau}{2}\Big)e^{-jm\tau t}\,dt\right|d\tau - N_0\right\}^2\\ &= \int_{-T}^{T}\int_{-T}^{T}\left|\frac{1}{2T}\int_{-T}^{T} E\Big[n\Big(t+\frac{\tau}{2}\Big)n^*\Big(t-\frac{\tau}{2}\Big)n^*\Big(t-t_1+\frac{\tau_1}{2}\Big)\right.\\ &\quad\left.\times\, n\Big(t-t_1-\frac{\tau_1}{2}\Big)e^{-jm(\tau-\tau_1)t}e^{-jm\tau_1 t_1}\Big]\,dt_1\right|d\tau\,d\tau_1 - N_0^2\\ &= \int_{-T}^{T}\int_{-T}^{T}\left|\frac{1}{2T}\int_{-T}^{T}\Big[N_0^2\delta(\tau)\delta(\tau_1)+N_0^2\delta\Big(\frac{\tau}{2}-\frac{\tau_1}{2}+t_1\Big)\delta\Big(\frac{\tau}{2}-\frac{\tau_1}{2}-t_1\Big)\Big]\right.\\ &\quad\left.\times\, e^{-jm(\tau-\tau_1)t}e^{-jm\tau_1 t_1}\,dt_1\right|d\tau\,d\tau_1 - N_0^2 = N_0^2 \end{aligned} \tag{80}$$

$$\begin{aligned}\mathrm{var}(\eta|H_1) &= E\left\{\int_{-T}^{T}\left|\frac{1}{2T}\int_{-T}^{T}\Big[n\Big(t+\frac{\tau}{2}\Big)+s\Big(t+\frac{\tau}{2}\Big)\Big]\right.\right.\\ &\quad\left.\left.\times\,\Big[n^*\Big(t-\frac{\tau}{2}\Big)+s^*\Big(t-\frac{\tau}{2}\Big)\Big]e^{-jm\tau t}\,dt\right|d\tau - (N_0+A)\right\}^2\\ &= 2AN_0+N_0^2 \end{aligned} \tag{81}$$

By using (76), we have (80) and (81) [26], shown at the top of the page. Inserting (78)–(81) into (33) yields (44).

ACKNOWLEDGMENT

The authors wish to thank Dr. Z. Bao for his valuable help and constructive input on this manuscript and Dr. B. W. Suter for his suggestions on the study of the resolution. The authors appreciate one of the anonymous reviewers for making many useful suggestions and Dr. S. Wang for reviewing preliminary drafts of this paper.

REFERENCES

[1] B. V. K. V. Kumar and C. W. Carroll, "Performance of the Wigner distribution function based detection methods," *Opt. Eng.*, vol. 23, no. 6, pp. 732–737, Dec. 1984.
[2] J. C. Wood and D. T. Barry, "Radon transformation of time-frequency distributions for analysis of multicomponent signals," *IEEE Trans. Signal Processing*, vol. 42, pp. 3166–3177, Nov. 1994.
[3] ——, "Tomographic time-frequency analysis and its application toward time varying filtering and adaptive kernel design for multicomponent linear-FM signals," *IEEE Trans. Signal Processing*, vol. 42, pp. 2094–2104, Aug. 1994.
[4] B. Boashash, "Time-frequency signal analysis," in *Advances in Spectral Estimation and Array Processing, vol. 1*, S. Haykin, Ed. Englewood Cliffs, NJ: Prentice-Hall, 1991, pp. 418–517, ch. 9.
[5] R. A. Altes, "Detection, estimation, and classification with spectrograms," *J. Acoust. Soc. Amer.*, vol. 67, pp. 1232–1246, Apr. 1980.
[6] M. Sanghadasa *et al.*, "Wavelet transform applied to synthetic aperture radar—Optimal implementation and adaptive techniques," *Opt. Eng.*, vol. 33, pp. 2282–2289, July 1994.
[7] M. Wang and Z. Bao, "Modified short-time Fourier transform," *Opt. Eng.*, vol. 34, pp. 1333–1337, May 1995.
[8] G. F. Boudreaux-Bartels, "Time-varying signal processing using the Wigner distribution," in *Advances of Geophysical Data Processing, vol. 2*, M. Simaan, Ed. Greenwich, CT: JAI, 1985.
[9] G. F. Boudreaux-Bartels and T. W. Parks, "Time-varying filtering and signal estimation techniques using Wigner distribution synthesis techniques," *IEEE Trans. Acoust., Speech, Signal Processing*, vol. ASSP-34, June 1986.
[10] G. F. Boudreaux-Bartels and P. J. Wiseman, "Wigner distribution analysis of acoustic well logs," in *Proc. IEEE ICASSP*, Dallas, TX, Apr. 1987.
[11] B. Bouachache and F. Rodriguez, "Recognition of time-varying signals in the time-frequency domain by means of the Wigner distribution," in *Proc. IEEE ICASSP*, San Diego, CA, Mar. 1984.
[12] S. Kay and G. F. Boudreaux-Bartels, "On the optimality of the Wigner distribution for detecting a chirp signal," in *Proc. IEEE ICASSP*, Mar. 1985.
[13] W. Li, "Wigner distribution method equivalent to dechirp method for detecting a chirp signal," *IEEE Trans. Acoust., Speech, Signal Processing*, vol. ASSP-35, Aug. 1987.
[14] H. J. Machale and G. F. Boudreaux-Bartels, "An algorithm for synthesizing signals from partial time-frequency methods using the cross Wigner distribution," *IEEE Trans. Signal Processing*, vol. 41, pp. 1986–1990, May 1993.
[15] F. Hlawatsch and W. Krattenthaler, "Two signal synthesis algorithms for pseudo Wigner distribution," in *Proc. IEEE ICASSP*, 1988, pp. 1550–1553.
[16] ——, "Bilinear signal synthesis," *IEEE Trans. Signal Processing*, vol. 40, pp. 352–363, Feb. 1992.
[17] P. M. Djuric and S. Kay, "Parameter estimation of chirp signals," *IEEE Trans. Acoust., Speech, Signal Processing*, vol. 38, pp. 2118–2126, Dec. 1990.
[18] B. Ristic and B. Boashash, "Kernel design for time-frequency signal analysis using the radon transform," *IEEE Trans. Signal Processing*, vol. 41, pp. 1996–2008, May 1993.
[19] I. Gradshteyn and I. Ryzhik, *Table of Integrals, Series, and Products.* San Diego, CA: Academic, 1980.
[20] C. E. Cook and M. Bernfeld, *Radar Signals: An Introduction to Theory and Application.* New York: Academic, 1967.
[21] D. E. Vakman, *Sophisticated Signals and the Uncertainty Principle in Radar.* New York: Springer-Verlag, 1968.
[22] L. Marple, "Resolution of conventional Fourier, autoregressive, and special ARMA methods of spectrum analysis," in *Proc. IEEE ICASSP*, Hartford, CT, May 1977.
[23] D. L. Jones and T. W. Parks, "A resolution comparison of several time-frequency representations," *IEEE Trans. Signal Processing*, vol. 40, pp. 413–420, Feb. 1992.
[24] M. P. Quirk, "Improving resolution for autoregressive spectral estimation by decimation," *IEEE Trans. Acoust., Speech, Signal Processing*, vol. ASSP-31, pp. 630–637, 1983.
[25] S. Barbarossa, "Analysis of multicomponent LFM signals by a combined Wigner–Hough transform," *IEEE Trans. Signal Processing*, vol. 43, June 1995.
[26] A. Papoulis, *Probability, Random Variables, and Stochastics Processes.* New York: McGraw-Hill, 1986.
[27] B. Boashash and P. O'Shea, "Polynomial Wigner–Ville distributions and their relationship to time varying high order spectra," *IEEE Trans. Signal Processing*, vol. 42, pp. 216–220, Jan. 1994.
[28] T. K. Bhattacharya and S. Haykin, "Application of time-varying distributions for improved radar target detection," in *Proc. ICASSP*, Apr. 1992, pp. 509–512.
[29] H. I. Choi and W. J. Williams, "Improved time-frequency representation

of multi-component signals using exponential kernels," *IEEE Trans. Signal Processing*, vol. 37, pp. 862–871, June 1989.
[30] P. J. Kootsooks *et al.*, "A unified approach to the STFT, TFD's and instantaneous frequency," *IEEE Trans. Signal Processing*, vol. 40, pp. 1971–1982, Aug. 1992.
[31] L. Stankovic, "A method for time-frequency analysis," *IEEE Trans. Signal Processing*, vol. 42, pp. 225–229, Jan. 1994.
[32] F. S. Cohen, S. Kadambe, and G. F. Boudreaux-Bartels, "Tracking of unknown nonstationary chirp signals using unsupervised clustering in the Wigner distribution space," *IEEE Trans. Signal Processing*, vol. 41, pp. 3085–3001, Nov. 1993.
[33] M. Wang, A. K. Chan, and C. K. Chui, "Linear frequency modulated signals detection using wavelet packets, ambiguity function and Radon transform," in *IEEE Antennas Propagat. Soc. Int. Symp.*, June 1995, pp. 308–311.
[34] L. B. Almeida, "The fractical Fourier transform and time-frequency representations," *IEEE Trans. Signal Processing*, vol. 42, pp. 3084–3091, Nov. 1994.
[35] A. W. Lohmann and B. H. Soffer, "Relationships between two transform: Radon–Wigner and fractical Fourier," *J. Opt. Soc. Amer.*, vol. A11, pp. 1798–1801, 1994.
[36] H. Urkowitz, *Signal Theory and Random Processes.* Dedham, MA: Artech House, 1983.
[37] R. R. Coifman and M. V. Wickerhauser, "Entropy based algorithms for best basis selection," *IEEE Trans. Inform. Theory*, vol. 38, pp. 713–718, 1992.
[38] C. K. Chui, Ed., *Wavelets: A Tutorial in Theory and Applications.* San Diego: Academic, 1992.
[39] M. Wang, A. K. Chan, and C. K. Chui, "Wigner–Ville distribution decomposition via wavelet packet transform," in *Proc. IEEE-SP Int. Symp. Time-Frequency Time-Scale Anal.*, Paris, France, June 1996.
[40] G. T. Herman, *Image Reconstruction from Projections: The Fundamentals of Computerized Tomography.* New York: Academic, 1980.
[41] N. G. DeBruijin, *Nieuw Archief voor Wiskunde XXI*, vol. 57, 1973.
[42] C. H. Chen, *Digital Waveform Processing and Recognition.* Boca Raton, FL: CRC, 1982.
[43] J. B. Thomas, *An Introduction to Statistical Communication Theory.* New York: Wiley, 1969.
[44] J. Brown and E. V. D. Glazier, *Signal Analysis.* New York: Rainhold, 1964.
[45] R. A. Smith, "The relative advantage of coherent and incoherent detectors: A study of their output noise spectra under various conditions," *Proc. Inst. Elect. Eng.*, vol. 98, pt. 4, 1951.
[46] H. R. Raemer, *Statistical Communication Theory and Applications.* Englewood Cliffs, NJ: Prentice-Hall, 1969.
[47] M. I. Skolnik, *Radar Handbook.* New York: McGraw-Hill, 1970.
[48] A. Papoulis, *Signal Analysis.* New York: McGraw-Hill, 1977.
[49] L. L. Scharf, *Statistical Signal Processing.* New York: Addison-Wesley, 1991.
[50] H. V. Poor, *An Introduction to Signal Detection and Estimation.* New York: Springer-Verlag, 1988.

Minsheng Wang was born in Xian, P.R. China, on October 13, 1967. He received the B.S. degree in 1988 and the M.S. degree in 1991, both in electrical engineering, from the Northwest Polytechnique University, P.R. China. He received the Ph.D. degree in 1994 in electrical engineering from Xidian University, P.R. China.

From 1994 to 1995, he held a postdoctoral position with the Department of Electrical Engineering, Texas A&M University, College Station, where his specialization was time–frequency signal analysis and the applications of wavelets to signal processing. His current research interests are digital signal processing and wavelets, spread spectrum communication (CDMA), and analog VLSI circuit design.

Andrew K. Chan (SM'89) received the Ph.D. degree in electrical engineering from the University of Washington, Seattle, in 1971.

He was on the faculty of Northern Arizona University, Flagstaff, from 1969 to 1976. He joined the faculty of Texas A&M University, College Station, in 1976 and is currently a Professor in the Department of Electrical Engineering. His broad research interest includes electromagnetic, acoustic, and optical wave propagation, soliton propagation, signal and image analysis, signal detection and recognition, and wavelet signal processing.

Dr. Chan is a member of Tau Beta Pi, Eta Kappa Nu, Sigmai Xi, and the Electromagnetic Academy.

Charles K. Chui (F'94) received the B.S. degree in applied mathematics, electrical engineering, and physics and the M.S. and Ph.D. degrees in mathematics, all from the University of Wisconsin, Madison, in 1962, 1963, and 1967, respectively.

He has been Distinguished Professor at Texas A&M University, College Station, since 1989, where he holds joint appointments in the Departments of Mathematics, Statistics, Computer Science, and Electrical Engineering. He is the author of more than 280 research papers and eight books and the editor of 12 volumes. His research interests include approximation theory, wavelets, and signal processing. He is Co-Editor-in-Chief (with R. R. Coifman and I. Daubechies) of the interdisciplinary journal *Applied and Computational Harmanic Analysis* with main focus on wavelets and applications.

Dr. Chui serves on the editorial boards of seven other journals and is Editor-in-Chief of two book series: *Wavelet Analysis and Its Applications* (New York: Academic) and *Approximations and Decompositions* (Singapore: World Scientific).